Energy materials

Li-In alloy: preparation, properties, wettability of solid electrolytes based on $Li_7La_3Zr_2O_{12}$

E. A. Il'ina[1,*] , K. V. Druzhinin[1,2], E. D. Lyalin[1,2], M. S. Plekhanov[3,4], I. I. Talankin[1,2], B. D. Antonov[1], and A. A. Pankratov[1]

[1] *Institute of High-Temperature Electrochemistry of Ural Branch of RAS, Akademicheskaya st., 20, Ekaterinburg, Russia 620137*
[2] *Ural Federal University Named After the First President of Russia B.N.Yeltsin, Mira st., 19, Ekaterinburg, Russia 620002*
[3] *Vyatka State University, Moskovskaya st., 36, Kirov, Russia 610000*
[4] *M.N. Mikheev Institute of Metal Physics of the Ural Branch of RAS, S. Kovalevskaya st., 18, Ekaterinburg, Russia 620108*

ABSTRACT

In the presented work, Li-In alloys with 10 and 18 at% Li were obtained. According to scanning electron microscopy, indium is evenly distributed in obtained alloys with different lithium contents. The atomic force microscopy study was used for elastic modulus investigation of Li-In alloys. It was established that obtained alloys are two-phase systems with matrix phase consisting of solid solution (α phase) and inclusions of the LiIn phase (β phase) with individual domain sizes of 0.5–3 μm. The wettability of the solid electrolyte based on $Li_7La_3Zr_2O_{12}$ with metallic In and Li-In alloy was study by high-temperature optical dilatometry. It was found that metallic indium wets ceramics better than obtained lithium–indium alloys. The symmetric cells with Li and Li-In alloy are assembled and studied. Li-In alloy application as an anode leads to significant reduction in the interface resistance between metallic anode and solid electrolyte from 37 to 0.4 kΩ cm^2 at room temperature. The composite solid electrolyte does not degrade in contact with Li-In anode.

Introduction

Currently, all-solid-state batteries are one of the most developed power sources [1, 2]. Because such batteries have a number of advantages in comparison with commercial lithium-ion batteries, for example, increased safety, a wider operating temperature range, and greater stability in case of depressurization. However, organization of optimal interface between solid electrolyte and electrodes is one of the main problems connected with all-solid-state batteries creation [1–5] since the anode, cathode and electrolyte are in a solid state. According to the literature data [3, 4, 6–8], compounds with a garnet-like structure based on $Li_7La_3Zr_2O_{12}$ (LLZ) are considered as promising solid electrolytes for application

---

Handling Editor: Kyle Brinkman.

Address correspondence to E-mail: ilyina@ihte.uran.ru

Springer

in high-energy power sources. LLZ has not only high values of lithium-ion conductivity, but also stability in contact with Li anode [4, 9]. But solid electrolytes based on LLZ is poorly wetted by metallic Li. Therefore, a low specific surface of the contact area between solid electrolyte and Li is formed. This, in turn, leads to high interfacial resistance and non-uniform current distribution during cell operation. Therefore, in recent years, active research has been carried out to solve this problem.

The insertion of various sintering additives, including glasses, into solid electrolytes based on the tetragonal and cubic $Li_7La_3Zr_2O_{12}$ is considered as one of the methods to improve the interfacial contact between electrolyte and electrode [10–15] because such modification of LLZ leads to decrease in the pores volume and thus to smoothing of electrolyte surface. In addition, this ceramic modification prevents the growth of lithium dendrites through the solid electrolyte during cell operation. Moreover, sputtering of a thin metal (or oxide) to form an intermediate conductive layer (known as SEI—Solid Electrolyte Interface) is considered by some researchers [4, 16, 17] for enhancing the interfacial contact in all-solid-state batteries. For example, in work [17], the problem of poor contact between metallic lithium and $Li_{6.4}La_3Zr_{1.4}Ta_{0.6}O_{12}$ solid electrolyte was solved by modifying the ceramic surface with a thin indium tin oxide interlayer; the interfacial resistance was reduced from 1192 to 32 Ω cm^2.

Lithium-based metal alloys application as anode materials can also be considered as one of the solution to the problems associated with high interface resistance, lithium dendrite formation and high reactivity of pure lithium [18–24]. Thus, for example, Li_xSi anode exhibits high specific capacity even with a small percentage of lithium ($Li_{4.4}Si$ shows the capacity of 2000 mAh) due to the ultra-high capacity of Si (4200 mAh g^{-1}). Also lithium alloys with other elements, for example Li-Sn and Li–Ge, are widely known as anode materials. Z. Tu et al. [19] developed batteries with Li-Sn hybrid anodes which possess high exchange currents and stable long-term characteristics. However, according to the literature reviews [22, 23], a volumetric change of the metal electrodes (especially based on Si, Sn) during the oxidation/reduction of lithium is the main disadvantage of their application. Some other elements, such as Na, Mg, Zn, In, Ag and Au, can also form alloys with lithium with certain properties [18]. In work [20], it was found that the introduction of 10 at% Mg into lithium metal anode can effectively prevent the loss of contact (formation of pores at the interface) between anode and solid electrolyte based on LLZ during electrochemical testing. The use of Li-Zn alloy also improved the contact between metallic anode and $Li_{6.28}Al_{0.24}La_3Zr_2O_{12}$ solid electrolyte, and, as a consequence, led to a decrease in the interface resistance [21].

Li-In alloy can be considered as perspective anode material, since it has a number of advantages, such as minimum capacity fade, high electropositivity of lithium in relative to indium and a constant redox potential of about 0.6 V vs. Li^+/Li^0 [18]. Moreover, Li-In alloy has a lower chemical activity in comparison with pure Li and keeps high rates of the electrochemical reaction Li^0/Li^+. According to Li–In phase diagram, the introduction of less than 50 at% Li does not lead to the compounds formation [24]. Some properties of Li-In electrode in electrochemical cells with liquid and Li_3PS_4 solid electrolyte were investigated by Santhosha A.L. et al. [24]. It was shown that electrode composition of the alloy with 44 at% lithium refers to the two-phase region ((In)–InLi). It was found that no significant changes occurred over 200 h (100 cycles) during cycling of the assembled symmetric cell. The obtained Li-In electrode exhibits good charge transfer kinetics as well as sufficient chemical stability in contact with Li_3PS_4 solid electrolyte. The increase in Li content in the Li-In alloy led to the stability problem of the selected solid electrolyte during cycling. Moreover, due to the presence of a large number of different phases in the lithium-rich region of the phase diagram, the redox potential can easily change after intercalation/deintercalation of lithium ions.

Thus, the Li-In alloy preparation, wettability study of solid electrolyte based on $Li_7La_3Zr_2O_{12}$ by Li-In alloy and the possibility of Li-In alloy application as anode for all-solid-state batteries creation are the aim of this work.

Materials and methods

Li_2CO_3, La_2O_3, $ZrO(NO_3)_2 \cdot 2H_2O$, $Al(NO_3)_3 \cdot 9H_2O$ were used as initial reagents for the sol–gel synthesis of $Li_7La_3Zr_2O_{12}$ with the addition of 0.15 mol of Al (LLZc). Lanthanum oxide was pre-dried at 1000 °C for 1 h to constant weight. The components were

mixed in the stoichiometric ratio, except Li_2CO_3, which was taken with the excess of 10 wt% [8]. These reagents were dissolved in the mixture of diluted HNO_3 and $C_6H_8O_7 \cdot H_2O$. The resulting solution was evaporated to transparent gel at 80 °C. Then, the obtained gel was dried and heated at ∼ 200 °C. The synthesis was performed by increasing the temperature stepwise (700 °C–1 h; 800 °C–1 h; 900 °C–1 h) in air atmosphere. Li_2CO_3, Y_2O_3 and SiO_2 were used as the starting materials in order to obtain $40.2Li_2O \cdot 5.7Y_2O_3 \cdot 54.1SiO_2$ (LYS) glass. The starting materials were taken in stoichiometric ratio and mixed. The mixture was heated in a platinum crucible for 1 h at 1500 °C. The samples were obtained by the conventional quenching method and were subsequently annealed below the glass transition temperature. LLZc with 1 wt% LYS glass was ground and homogenized in a planetary mill (FRITSCH, Germany) with agate balls of 10 mm in diameter (the mass ratio between the balls and the product was 3:1). The grinding was performed in 5 ml of ethanol per 10 g of the product at a speed of 750 rpm during 30 min. Then, the obtained powder was cold-pressed into pellets (diameter 10 mm and thickness ∼ 0.8 mm) at 240 MPa. The pellets were covered with powder of the same composition and then sintered at 1150 °C for 1 h on a Pt substrate in Air atmosphere.

The preparation of In-Li alloy with 10 and 18 at% Li was carried out by melting of Li and In at a temperature of ∼ 300 °C. Firstly, metallic In was melted in a beryllium crucible on a heated plate C-MAG HP 7 (IKA, Germany), then the required weighed amount of lithium metal was added. The resulting melt was heated in a furnace to 700 °C with holding for 1 h to homogenize the alloy. Then, the obtained melt was cooled to room temperature.

The wettability investigation of the solid electrolytes based on $Li_7La_3Zr_2O_{12}$ by In and Li-In alloy was carried out using a high-temperature optical dilatometer ODP 868 (TA Instruments, USA) in the temperature range of 20–300 °C in air.

Metallic Li and Li-In alloy was rolled to the foil, electrodes were cut out from obtained foil and adpressed by rolling to both surfaces of the sample (the diameter of electrodes are equal ∼ 5 mm). The symmetric cells were assembled in a dry argon box M-BROWN (H_2O concentration < 1 ppm). The electrical resistance of the solid electrolyte and symmetric cells with Li and Li-In alloy was measured by electrochemical impedance spectroscopy. The measurements were carried out using a potentiostat–galvanostat P-5X (Elins, Russia) in the 0.001–500 kHz frequency range at 25, 130 and 200 °C. All operations were made in an argon-filled isolated cage [25].

The phase composition of the obtained materials was examined by X-ray diffraction method (XRD) using a Rigaku D/MAX-2200VL/PC diffractometer (Rigaku, Japan) with monochromate CuKα radiation over a 2θ range of 10–80° at room temperature.

Li-In alloys were studied by the scanning electron microscopy (SEM) using an autoemission electron microscope TESCAN MIRA 3 LMU (TESCAN, Czech Republic). The maps of the elements distribution on the surface of Li-In alloys (EDAX) were compiled using the energy-dispersive X-ray microanalysis.

Li-In alloy was analyzed under atomic-force microscopy (AFM) using an NTEGRA Aura (NT-MDT Spectrum Instruments, Russia) microscope. HA-HR/Pt ETALON probe with cantilever length of 123 μm was used. Spring vibrance frequency is 230 kHz and stiffness is 17 N/m. Scanning was performed in hybrid mode with rate of 1 Hz, and the field area was 10 × 10 μm with resolution of 10 × 10 nm.

## Result and discussion

Materials characterization

Solid electrolyte

The cubic modification of $Li_7La_3Zr_2O_{12}$ stabilized by aluminum as well as the composite electrolyte based on it with 1 wt% LYS glass addition (LLZc + 1 wt% LYS) were synthesized as solid electrolytes [26]. XRD patterns of obtained solid electrolytes are shown in Fig. 1a. According to the obtained data, solid electrolytes have cubic structure with space group Ia-3d, which is typical for compounds with a garnet-like structure [4]. It should be noted that no impurity phases were observed. The temperature dependences of total conductivity for the investigated solid electrolytes are shown in Fig. 1b. The total lithium-ion conductivity at 25 °C for the LLZc and the composite based on it were equal to 1.5×10^{-4} and 2.8×10^{-4} S cm^{-1}, respectively.

Figure 1 XRD patterns (**a**) and Arrhenius plots for total conductivity (**b**) of LLZc and LLZc + 1 wt% $40.2Li_2O \cdot 5.7Y_2O_3 \cdot 54.1SiO_2$ solid electrolytes.
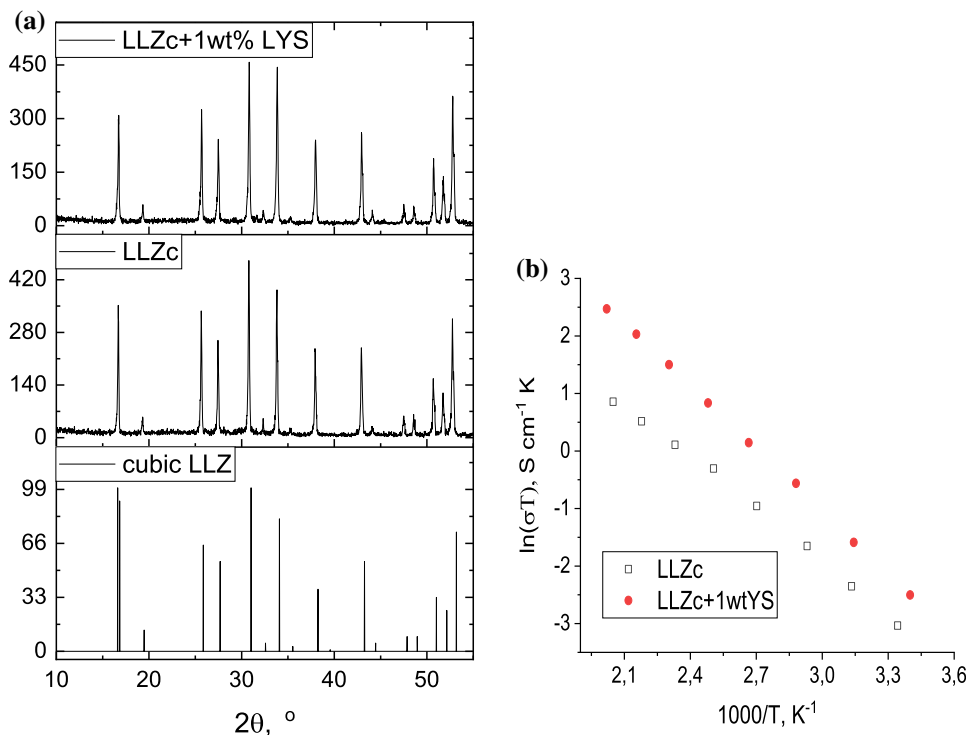
Li-In alloy

The obtaining alloys contain a small amount of lithium; therefore, their diffraction patterns are close to metallic indium according to the XRD data (Fig. 2). However, some change of the peak intensity is observed with an increase in lithium content. These data indicate a slight change in the alloy composition.

The surface of the metal alloys was studied using SEM (Fig. 3). It was established using the EDAX maps that indium is evenly distributed in alloys with different lithium contents (Figs. 3b, d). Unfortunately, distribution of lithium in studied samples cannot be determined using this technique. Nevertheless, the absence of depleted and enriched areas of indium confirms the formation of a homogeneous alloy, without any impurities, as well as XRD data.

Figure 4 shows topology map and elastic modulus distribution over the Li-In alloy (18 at% Li) surface region. Elastic modulus distribution map was recorded in single run tapping mode using signal mismatch technique. The sample under investigation was prepared as a 100 μm foil on molybdenum substrate, by use of stainless steel calendar. Figure 3 shows the SEM images of alloys foils, and one can see that no phase segregation occurred. Topology map shown in Figs. 4 a and b shows that the foil possess
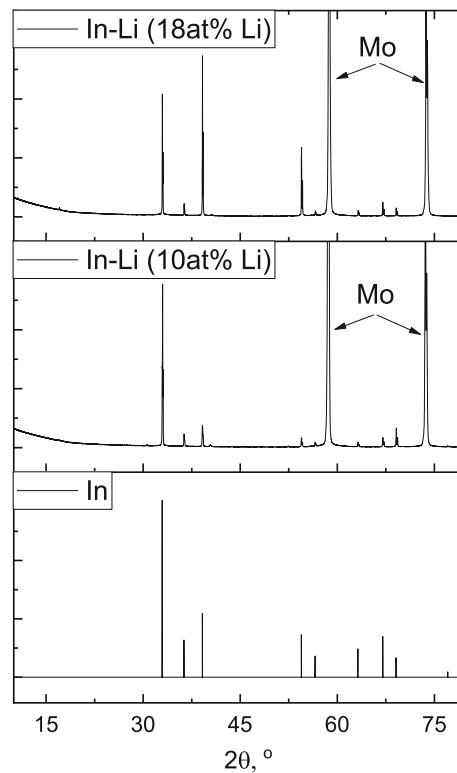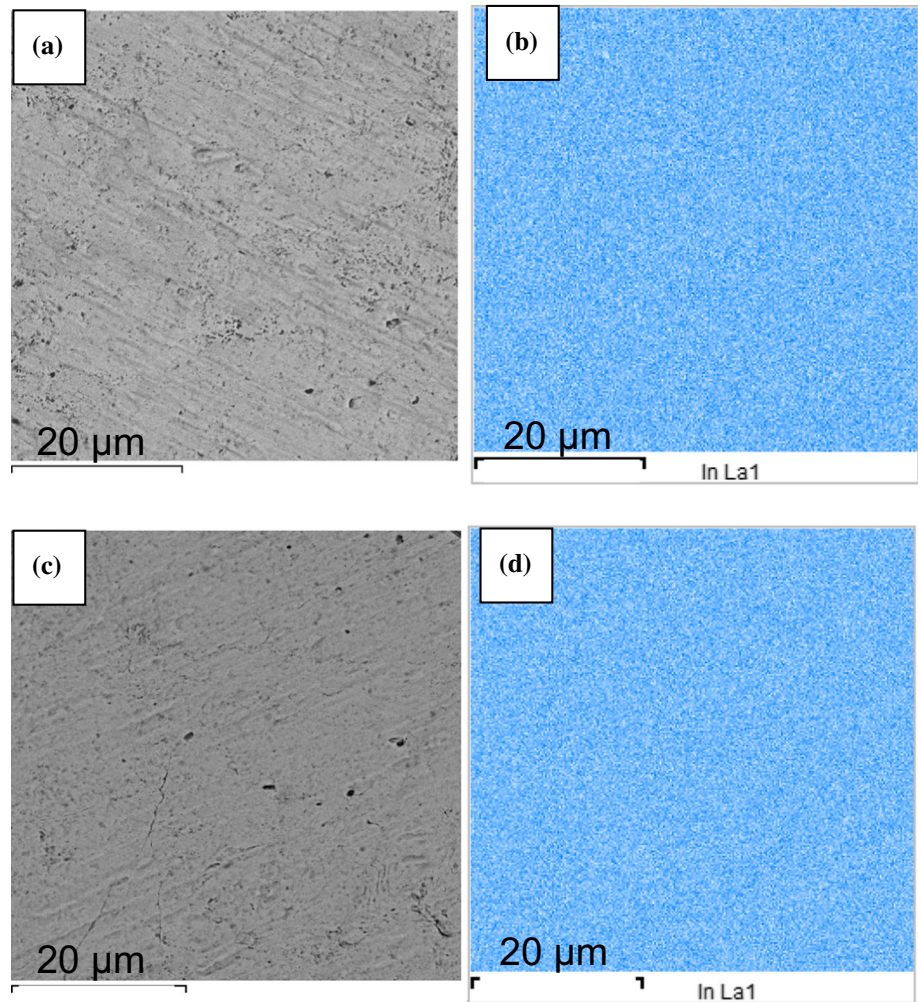
Figure 2 XRD patterns of Li-In alloy with 10 and 18 at% Li.

rugosity up to 500 nm pointing at high plasticity of rolled alloys. Alloy foils easily adhered to

Figure 3 SEM images of Li-In alloys with 10 (**a**) and 18 at% Li (**c**) and a map of distribution of indium (EDAX) on the samples surface (**b**, **d**), respectively.

molybdenum substrate and stainless steel cylinder under rolling, so the rugosity emerged at rolled foil exfoliation from cylinder.

Elastic modulus distribution map (Fig. 4c) shows the presence of two clearly separated domain regions. The dominating one is continuous matrix characterized by Young modulus value of 3.5–4.0 GPa. Minor domain phase is a quantity of randomly distributed domains with sizes of 0.5–3.0 μm characterized by Young modulus values of 3.0–3.2 GPa. Pure lithium metal is known to possess elastic modulus of around 5.0 GPa, and pure indium has the value of around 11.0 GPa [27]. It means that no one domain represents pure metal inclusions, the obtained alloys represent themselves binary systems and both phases are Li-In compounds.

The phase diagram of Li-In system shows the presence of several stable compositions in lithium-rich region [28]. The only way of phase separation for compositions with 10 or 18 at% of Li at temperatures below 158.7 °C is disproportion of lithium and indium content in α and β phases. The authors of [28] state that Li-In solid solution area in In-rich region is very narrow and point the estimated value of maximal lithium dissolved in metallic indium as 1.5 at%, and the solid solution is marked as α phase. The other phase is LiIn composition with varied content, at low temperatures estimated as 47 at% of Li. The β phase possesses the structure close to initial In with deviations in lattice parameters of not higher than 0.03 Å.

Thus, the obtained alloys represent themselves as two-domain structure of α and β phases. To find out the dominant phase, we estimated phase content via Eq. (1):

$$n \cdot A + (100 - n) \cdot B = X(AB : \chi_1, (100 - \chi_1)) + (1 - X) \cdot (AB : \chi_2, (100 - \chi_2))$$
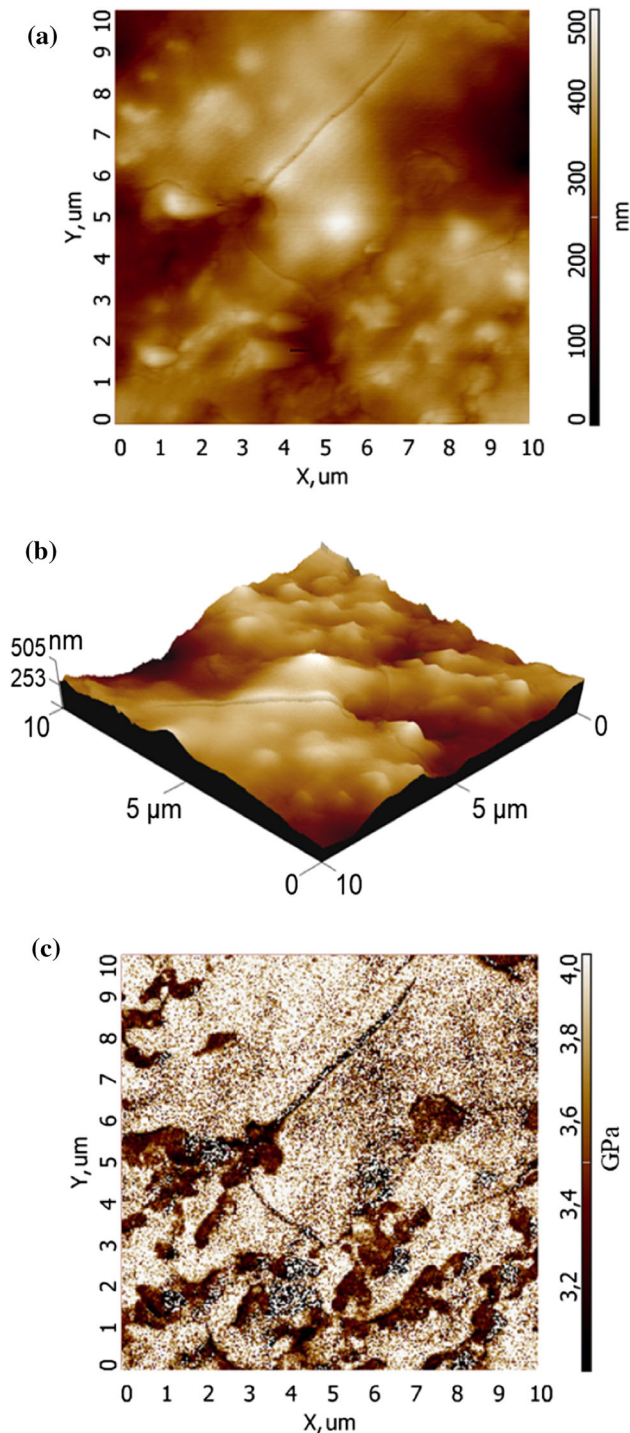
Figure 4 Topology of the surface of the In-Li (18 at% Li) alloy region (**a** and **b**), and Young modulus (**c**) map, obtained using the atomic-force microscope.

$$X = \frac{n - \chi_2}{\chi_1 - \chi_2} \qquad (1)$$

where X is molar portion of first phase of binary system AB composed from two initial atom species A and B; n is molar percent of A content in initial mixture (A + B); χ_1 is molar percent of A content in first phase composition after disproportion; χ_2 is molar percent of A content in second phase after disproportion.

The samples of Li-In alloy with 18 at% Li and 82 at% In are estimated to be composed of 64 mol% of solid solution (α phase) and 36 mol% of β phase LiIn. The samples of Li-In alloy with 10 at% of Li and 90 at% In are estimated to be composed of 81 mol% of solid solution (α phase) and 19 mol% of β phase LiIn. The real content of alloys might slightly deviate from estimated values because of lithium losses under the preparation procedure, but the absence of lithium oxide or carbonate peaks on XRD patterns (see Fig. 2) supports the main conclusion that Li-In solid solution is the dominating phase in both alloys. Thus, the alloy structure is β phase domain inclusions in solid solution of Li in In.

One should note that both solid solution phase and β phase LiIn are characterized by room temperature elastic modulus values (∼ 4.0 GPa and ∼ 3.2 GPa, respectively) lower than pure metals possess. That coincides with their heightened plasticity noticed at foils preparation. This fact means facilitated technological treatment of alloys in contrast to indium and lithium.

Wettability of the solid electrolytes surface by In and Li-In alloy

The wettability of the solid electrolytes based on $Li_7La_3Zr_2O_{12}$ surface by metallic indium was investigated. From Fig. 5, it can be seen that metallic indium after melting (> 156 °C [20]) wets the surface of the studied samples, but does not flow over it. The softening of indium was observed at ∼ 124 °C. The calculated contact angles for LLZc and LLZc + 1 wt% LYS solid electrolytes are equal to 77 and 57°, respectively. So the composite based on cubic LLZ can be considered as promising solid electrolyte for power sources with In-based anode.

The wettability of the composite electrolyte surface by Li-In alloys with different Li content was also studied. During heating, the softening of alloys with 10 and 18 at% Li was observed at higher temperatures–136 and 140 °C, respectively. Figure 6 shows that obtained alloys wet the solid electrolyte worse than metallic indium. The calculated contact angles by Li-In alloys (with 10 and 18 at% Li content) are

Figure 5 Wettability of the LLZc (**a**, **b**) and LLZc + 1 wt% $40.2Li_2O \cdot 5.7Y_2O_3 \cdot 54.1SiO_2$ (**c**, **d**) solid electrolytes by metallic In at 22 and 200 °C.
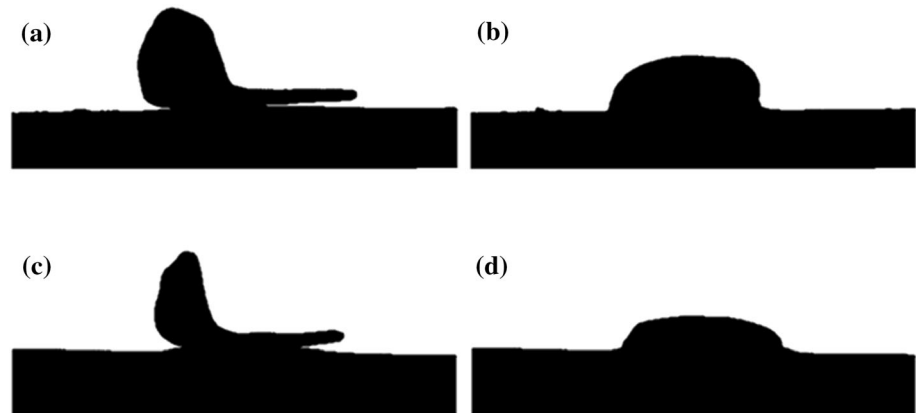
equal 103 and 112°, respectively. However, the alloy has a good adhesion to LLZ-based electrolyte, and it was difficult to remove Li-In alloy from solid electrolyte surface. Moreover, it was shown in work [29] that metallic lithium rolls into a drop after melting on the LLZ surface. Therefore, the Li-In alloy application instead of metallic Li can have a positive effect on reducing the resistance between solid electrolyte and anode in all-solid-state batteries.
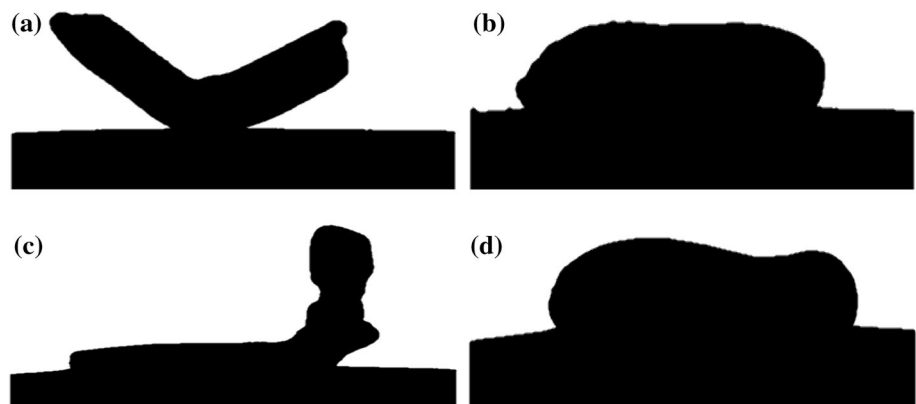
Symmetric cells with Li and Li-In anode

The impedance plots of Li | LLZc + 1 wt% LYS | Li symmetric cell are shown in Fig. 7a. The resistance of the symmetric cell was determined from the intersection of the arc with the real part of the impedance value Z′. Figure 7a also shows an equivalent circuit, according to which the total cell resistance is the sum of the resistance of the electrolyte (R_{el}) and the resistance at the interface between the Li electrodes and the solid electrolyte (R_1). The interfacial resistance of the symmetric cells was calculated by dividing the low-frequency semicircle diameter by a

factor of two, as the total interfacial resistance corresponds to two symmetric interfaces. It should be noted that the resistance of composite solid electrolyte is only a few hundred of Ω, while the resistance at the Li | LLZc + 1 wt% LYS interface is equal to $\sim$ 37 kΩ cm^2. Such high values of the interfacial resistance related to the poor wettability of the LLZc + 1 wt% LYS solid electrolyte with lithium. Obtained values of electrolyte resistance coincide with the ones recorded on symmetric cell In | LLZc + 1wt% LYS | In (Figure S1a).

The Li-In alloy application significantly reduced the total resistance of symmetric cells even at room temperature (Figs. 7b, c). It should be noted that Li-In alloy is a rather ductile material that is well-applied to ceramics. The Li replacement by Li-In alloy leads to decrease in the interface resistance between anode and solid electrolyte from 37 to 0.4 kΩ cm^2. Figure 7b also represents the equivalent electrical circuit used for fitting all the spectra for symmetric cell with Li-In alloy. It was found that the minimal amount of CR elements should be two. Thus, the extra-CR element should be connected to the process at the Li-In |

Figure 6 Wettability of the LLZc + 1 wt% $40.2Li_2O \cdot 5.7Y_2O_3 \cdot 54.1SiO_2$ solid electrolyte by Li-In alloy with 10 (**a**, **b**) and 18 at% Li (**c**, **d**) at 22 and 200 °C.
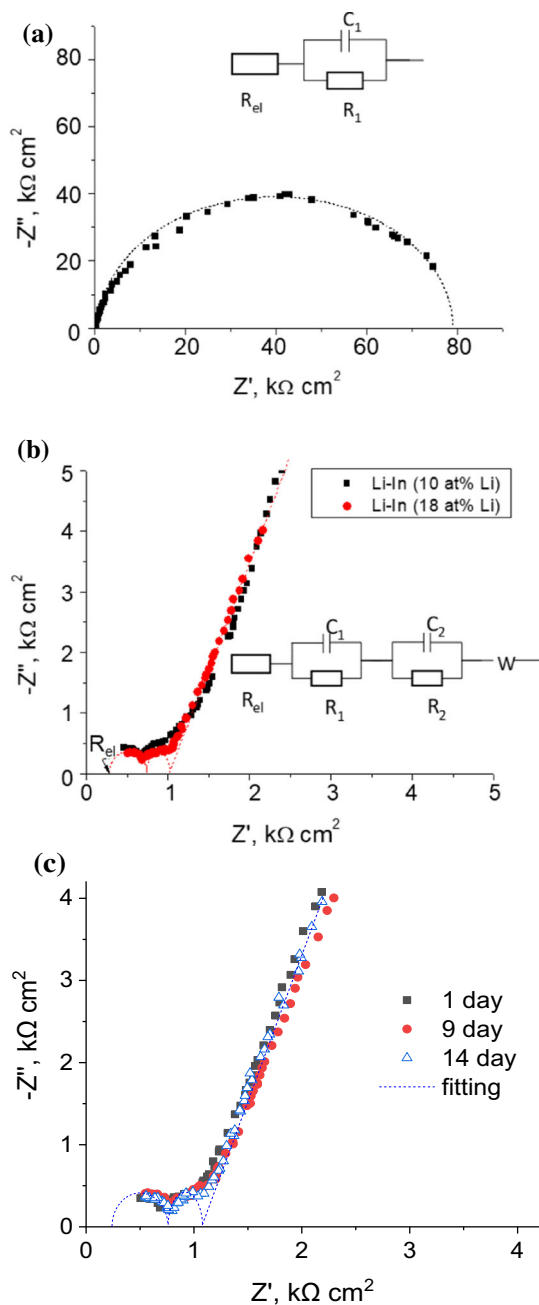
Figure 7 Impedance plots of the Li | LLZc + 1 wt% LYS | Li (a) and Li-In | LLZc + 1 wt% LYS | Li-In (b, c) symmetric cells at 25 °C.

LLZc + 1 wt% LYS interface. The resistances of symmetric cells with different Li content in the Li-In alloy have similar values (Fig. 7b). This fact also confirms that the CR of the elements is related to the processes at the interface. It should be noted that the average resistance of assembled symmetric cells does not change significantly for 14 days (Fig. 7c).

Moreover, the symmetrical cells were heated, and their resistance at 130 and 200 °C was measured. Figure 8 shows that an increase in temperature leads to a decrease in the total resistance of the Li-In | LLZc + 1 wt% LYS | Li-In symmetric cell. The total resistance of the symmetric cell and Li-In | LLZc + 1 wt% LYS interface resistance at 200 °C are equal to ∼ 68 and 31 Ω cm^2, respectively. In case of symmetric cell, In | LLZc + 1wt% LYS | In impedance spectroscopy gave slightly more total cell resistance values—2000 and 120 Ω cm^2 at 130 and 200 °C, respectively (Figure S1b). It was interesting to determine the effect of the preheating on the resistance of studied symmetrical cell. It was established that after cooling to room temperature, the resistance of the Li-In | LLZc + 1 wt% LYS | Li-In symmetric cells decreased to the values of initially assembled cells. This fact also confirms the good adhesion of the Li-In alloy to the composite solid electrolyte based on LLZ. So, preliminary heat treatment does not lead to an improvement of interfacial resistance assembled cells with Li-In alloy.

Fitting the spectra of studied cells with Li-In (10 and 18 at% Li) alloy with the proposed equivalent circuit (Fig. 7b) yields the results collected in Table 1. It can be seen that R_1 decreases gradually with temperature, while R_2 decreases slightly after heating to 130 °C. A further increase in temperature leads to a sharper decrease in R_2, which is possibly associated with softening of the Li-In alloy. Thus, the decrease in the interface resistance between anode and solid electrolyte from 420 to 31 Ω cm^2 was observed after heating to 200 °C. Table 1 summarizes resistance values (R_{el}, R_1 and R_2) driven from impedance
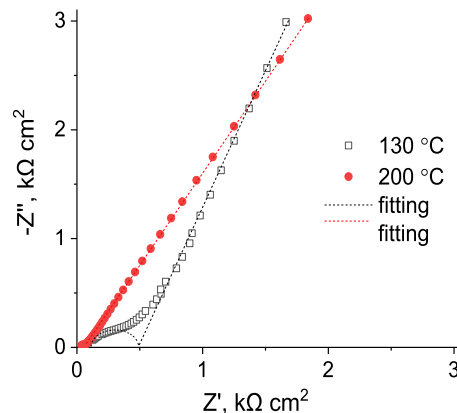

Figure 8 Impedance plots of the Li-In | LLZc + 1 wt% LYS | Li-In symmetric cells at 130 and 200 °C.

Table 1 Resistance values from fitting impedance plots of Li-In|LLZc + 1 wt% LYS|Li-In symmetric cells

t, °C	R_{el}, Ω cm^2		R_1, Ω cm^2		R_2, Ω cm^2	
	10 at% Li	18 at% Li	10 at% Li	18 at% Li	10 at% Li	18 at% Li
25	280	275	480	490	340	345
130	16	16	104	100	320	330
200	6	6	26	25	36	38

spectroscopy data (Figs. 7, 8). Electrolyte resistance (R_{el}) in all cases is defined as low-resistance R value fitting the first arc (the plot starts at $Z' > 0$). The value at 25 °C coincides with the one obtained by impedance spectroscopy with GaAg electrodes. R_{el} values at high temperatures (130 and 200 °C) are obtained in experiment with GaAg electrodes, as we cannot precisely identify the intersection point corresponding to R_{el} in case of Li-In electrodes applied (Fig. 8) because the impedance data describing this part of plot shift to more high-frequency region out of instrument limitations. These data were obtained via experiment at symmetric cells with GaAg electrodes.

The symmetric cells were disassembled in a box with the argon atmosphere after the experiments. It should be noted that the Li-In alloy retained its metallic luster and the surface of the studied samples did not change color. Li-In alloy was removed from the studied sample for an investigation of the solid electrolyte surface by XRD analysis. XRD patterns of composite electrolyte surface before and after contact with Li-In alloy are shown in Figure S2. According to XRD data, the formation of any impurities after heating symmetric cells to 200 °C was not detected. So, it can be concluded that the degradation of the solid electrolyte after contact with Li-In anode was not occurred.

Conclusions

Li-In alloys with 10 and 18 at% Li were obtained by melting of In and Li metals. Using SEM study, it was found that indium is evenly distributed in alloys with different lithium contents, and there are no areas of pure metals. The elastic modulus of Li-In alloys were investigated using the AFM study. It was established that obtained alloys are two-phase systems with matrix phase consists of solid solution (α phase) and inclusions of the LiIn phase (β phase) with individual domain sizes of 0.5—3 μm. Both phases are characterized by lower elastic modulus values compared to

the pure metals, and the obtained material has a higher plasticity. High-temperature optical dilatometry was used to study the wettability of the solid electrolyte based on $Li_7La_3Zr_2O_{12}$ with metallic In and Li-In alloy. It was found that metallic indium wets ceramics better than obtained lithium–indium alloys; however, Li-In alloy has good adhesion to the composite solid electrolyte.

The Li|LLZc + 1 wt% LYS|Li and Li-In|LLZc + 1 wt% LYS|Li-In symmetric cells were assembled, and their resistance was measured at room temperature and elevated. It was found that the Li-In alloy application as an anode leads to significant reducing the total resistance of the assembled cell at 25 °C. The decrease in the interface resistance between anode and solid electrolyte from 37 to 0.4 kΩ cm^2 was observed because of Li replacement by Li-In alloy. An increase in temperature led to the decrease in the total resistance of symmetric cells. It was established that the composite solid electrolyte is stable in contact with Li-In anode. Thus, the possibility of Li-In alloy application was shown in order to optimize the interface between anode and composite electrolyte based on $Li_7La_3Zr_2O_{12}$ for all-solid-state batteries creation.

Declarations

Conflict of interest The authors declare that they have no conflict of interest.

Supplementary Information: The online version contains supplementary material available at https://doi.org/10.1007/s10853-021-06645-z.

References

[1] Kim JG, Son B, Mukherjee S, Schuppert N, Bates A, Kwon O, Choi MJ, Chung HY, Park S (2015) A review of lithium and non-lithium based solid-state batteries. J Power Sources 282:299–322. https://doi.org/10.1016/j.jpowsour.2015.02.054

[2] Chen L, Huang YF, Ma J, Ling H, Kang F, He YB (2020) Progress and perspective of all-solid-state lithium batteries with high performance at room temperature. Energy Fuels 34:13456–13472. https://doi.org/10.1021/acs.energyfuels.0c02915

[3] Subramanian K, Alexander GV, Karthik K, Patra S, Indu MS, Sreejith OV, Viswanathan R, Narayanasamy J, Murugan R (2021) A brief review of recent advances in garnet structured solid electrolyte based lithium metal batteries. J Energy Storage 33:102157. https://doi.org/10.1016/j.est.2020.102157

[4] Ramakumar S, Deviannapoorani C, Dhivya L, Shankar LS, Murugan R (2017) Lithium garnets: Synthesis, structure, Li^+ conductivity, Li^+ dynamics and applications. Prog Mater Sci 88:325–411. https://doi.org/10.1016/j.pmatsci.2017.04.007

[5] Duan H, Oluwatemitope F, Wu S, Zheng H, Zou Y, Li G, Wu Y, Liu H (2020) Li/Garnet Interface Optimization: An Overview. ACS Appl Mater Interfaces 12:52271–52284. https://doi.org/10.1021/acsami.0c16966

[6] Kammampata SP, Thangadurai V (2018) Cruising in ceramics – discovering new structures for all-solid-state batteries – fundamentals, materials, and performances. Ionics 24:639–660. https://doi.org/10.1007/s11581-017-2372-7

[7] Yaroslavtsev AB (2016) Solid electrolytes: Main prospects of research and development. Rus Chem Rev 85:1255–1276. https://doi.org/10.1070/rcr4634

[8] Abdulai M, Dermenci KB, Turan S (2021) Lanthanide doping of Li7La3-xMxZr2O12 (M=Sm, Dy, Er, Yb; x=0.1–1.0) and dopant size effect on the electrochemical properties. Ceram Int 47:17034–17040. https://doi.org/10.1016/j.ceramint.2021.03.010

[9] Murugan R, Thangadurai V, Weppner W (2007) Fast lithium ion conduction in garnet-type $Li_7La_3Zr_2O_{12}$. Angew Chem Int Ed 46:7778–7781. https://doi.org/10.1002/anie.200701144

[10] Janani N, Deviannapoorani C (2014) Influence of sintering additives on densification and Li^+ conductivity of Al doped $Li_7La_3Zr_2O_{12}$ lithium garnet. RSC Adv 4:51228–51238. https://doi.org/10.1039/C4RA08674K

[11] Rosero-Navarro NC, Yamashita T, Miura A, Higuchi M, Tadanaga K, Stevenson JW (2016) Effect of sintering additives on relative density and Li-ion conductivity of Nb-doped $Li_7La_3ZrO_{12}$ solid electrolyte. J Am Ceram Soc 100:276–285. https://doi.org/10.1111/jace.14572

[12] Tang Y, Zhang Q, Luo Z, Liu P, Lu A (2017) Effects of $Li_2O-Al_2O_3-SiO_2$ system glass on the microstructure and ionic conductivity of $Li_7La_3Zr_2O_{12}$ solid electrolyte. Mater Lett 193:251–254. https://doi.org/10.1016/j.matlet.2017.01.134

[13] Xu B, Li W, Duan H, Wang H, Guo Y, Li H, Liu H (2017) Li_3PO_4-added garnet-type $Li_{6.5}La_3Zr_{1.5}Ta_{0.5}O_{12}$ for Li-dendrite suppression. J Power Sources 354:68–73. https://doi.org/10.1016/j.jpowsour.2017.04.026

[14] Xue W, Yang Q, Li S, Liu Y, Wang L, Cheng R, Chen C (2020) The effect of LiAlSiO4 additions on lithium ionic conductivity of garnet Li6.75La3Zr1.75Nb0.25O12 prepared by solid-state synthesis. Solid State Ionics 350:115313. https://doi.org/10.1016/j.ssi.2020.115313

[15] Patra S, Narayanasamy J, Chakravarty S, Murugan R (2020) Higher critical current density in lithium garnets at room temperature by incorporation of an Li4SiO4-related glassy phase and hot isostatic pressing. ACS Appl Energy Mater 3:2737–2743. https://doi.org/10.1021/acsaem.9b02400

[16] Bai L, Xue W, Li Y, Liu X, Li Y, Sun J (2018) The interfacial behaviors of all-solid-state lithium ion batteries. Ceram Int 44:7319–7328. https://doi.org/10.1016/j.ceramint.2018.01.190

[17] Lou J, Wang G, Xia Y, Liang C, Huang H, Gan Y, Tao X, Zhang J, Zhang W (2020) Achieving efficient and stable interface between metallic lithium and garnet-type solid electrolyte through a thin indium tin oxide interlayer. J Power Sources 448:227440. https://doi.org/10.1016/j.jpowsour.2019.227440

[18] Gu X, Dong J, Lai C (2020) Li-containing alloys beneficial for stabilizing lithium anode: A review. Engineering Reports. https://doi.org/10.1002/eng2.12339

[19] Tu Z, Choudhury S, Zachman MJ, Wei S, Zhang K, Kourkoutis LF, Archer LA (2018) Fast ion transport at solid-solid interfaces in hybrid battery anodes. Nat Energy 3(4):310–316. https://doi.org/10.1038/s41560-018-0096-1

[20] Krauskopf T, Mogwitz B, Rosenbach C, Zeier WG, Janek J (2019) Diffusion limitation of lithium metal and Li–Mg alloy anodes on LLZO type solid electrolytes as a function of

temperature and pressure. Adv Energy Mater. https://doi.org/10.1002/aenm.201902568

[21] Alexander GV, Sreejith OV, Indu MS, Murugan R (2020) Interface-compatible and high-cyclability lithiophilic lithium-zinc alloy anodes for garnet-structured solid electrolytes. ACS Appl Energy Mater 3:9010–9017. https://doi.org/10.1021/acsaem.0c01430

[22] Park C-M, Kim J–H, Kim H, Sohn H–J, (2010) Li-alloy based anode materials for Li secondary batteries. Chem Soc Rev 39:3115–3141. https://doi.org/10.1039/b919877f

[23] Obrovac MN, Chevrier VL (2014) Alloy Negative Electrodes for Li-Ion Batteries. Chem Rev 114:11444–11502. https://doi.org/10.1021/cr500207g

[24] Santhosha AL, Medenbach L, Buchheim JR, Adelhelm P (2019) The Indium-Lithium electrode in solid-state lithium ion batteries: Phase formation, redox potentials and interface stability. Batteries Supercaps 2:524–529. https://doi.org/10.1002/batt.201800149

[25] Il'ina EA, Druzhinin KV, Antonov BD, (2020) Stability of composite electrolytes based on $Li_7La_3Zr_2O_{12}$ to metallic lithium. Ionics 26:163–172. https://doi.org/10.1007/s11581-019-03177-0

[26] Il'ina EA, Druzhinin KV, Antonov BD, Pankratov AA, Vovkotrub EG, (2019) Influence of Li_2O–Y_2O_3–SiO_2 glass additive on conductivity and stability of cubic $Li_7La_3Zr_2O_{12}$. Ionics 25:5189–5199. https://doi.org/10.1007/s11581-019-03077-3

[27] Cardarelli F. 2018 Materials handbook, Springer, 2254 p., doi: https://doi.org/10.1007/978-3-319-38925-7_4.

[28] Alexander WA, Calvert LD, Gamble RH, Schinzel K (1976) The lithium-indium system. Can J Chem 54:1052–1060. https://doi.org/10.1139/v76-150

[29] Fu KK, Gong Y, Liu B, Zhu Y, Xu S, Yao Y, Luo W, Wang C, Lacey SD, Dai J, Chen Y, Mo Y, Wachsman E, Hu L (2017) Toward garnet electrolyte-based Li metal batteries: An ultrathin, highly effective, artificial solid-state electrolyte/metallic Li interface. Sci Adv 3:e1601659. https://doi.org/10.1126/sciadv.1601659